MODIFIED CYCLIC MODEL OF INTERFACES WITH ROUGHENED SURFACE AND DOWEL BAR SUBJECTED TO NORMAL AND SHEAR STRESSES

YUYA TAKASE[*], TAIZO YAMADA[†] AND TAKAHIDE ABE[††]

[*] College of Design and Manufacturing Technology, Muroran Institute of Technology,
Mizumoto 27-1, Muroran, Japan
e-mail: y.takase@mmm.muroran-it.ac.jp

[†] College of Environmental Technology, Muroran Institute of Technology
Mizumoto 27-1, Muroran, Japan
e-mail: yamada.taizo@tohata.co.jp

[††] Institute of Technology, Tobishima Corporation
Kimagase 5472, Noda, Japan
e-mail: takahide.abe@tobishima.co.jp

Key words: Reinforced concrete, Seismic retrofit, Roughened concrete interface, Dowel action

Abstract: When reinforced concrete (RC) buildings are seismically retrofitted, new members are attached to existing members through interfaces with roughened surfaces using vibratory hammer and post-installed dowel bars. To attach extended members to the outside of an existing frame, the interfaces are subjected to bending moments and shear forces. In other words, interfaces are subjected to the compressive or tensile normal stresses in addition to shear stresses. However, the previous literature is limited in its investigation of the behaviors under such combined stresses. Therefore, in the authors' previous study, the shear strength estimation of the interfaces was proposed; and then, the cyclic model was presented. Although the proposed model can be applied to the interfaces subjected to tensile and shear stresses, the behavior under compressive normal stress was not discussed. Hence, in this study, the model was improved to estimate the cyclic behavior under the different normal stresses. The Saenz model, which is a constitutive law of concrete, was used to evaluate the envelope behavior. In addition, the peak stress was calculated by using the proposed estimation. For the compressive normal stress, the envelope model and peak stress were modified. Subsequently, the proposed cyclic rules were applied; and, a previous dowel model was incorporated into the modified model. The concrete compressive strength was set to 20-23 N/mm^2, the diameters of the anchor bar were 13, 16, and 19 mm, the compressive normal stress was set to –0.48 N/mm^2, and the tensile ratio r_N was set to 0.00, 0.33, and 0.66. Epoxy adhesive was used. As a result, the modified model agreed well with the test results; the average ratio of the test results to the model results was 0.91-1.12. In addition, with the increase of δ, the effect of the dowel bar was intensified; whereas, under the compressive normal stress, it became insignificant. Finally, it was concluded that the modified model could reasonably estimate the behavior under the various stresses.

1 INTRODUCTION

In recent years, the importance of sustainable development goals (SDGs) and decarbonization have been increasing.

Therefore, seismic retrofit is important to use seismically week concrete structures. When new members are connected to existing members, the concrete surface is roughened and post-installed dowel bars are applied to the

surface. For reinforced concrete (RC) buildings, the roughened surfaces are produced using a vibratory hammer. **Fig. 1** illustrates the interfaces between new and existing members. During an earthquake, the interfaces are subjected to shear and normal forces.

In the previous studies, the concrete interfaces and the dowel action are traditional topics. The shear-friction theory was proposed by Mattock [3] in the 1960s. Since the 1980s, the aggregate interlocking has been studied by Walraven et al. [4-5] and Bujadaham [6-7]. Furthermore, many researchers have studied dowel action. Dowel action was started by Friberg [8]. Vintzēleou and Tassios proposed the famous dowel formula. [9] Sorensen introduced catenary actions to dowels. [10]

Moreover, the authors studied a roughened surface by a hammer and post-installed dowel bars. [1-2,11-16]. In the studies, the interfaces and the post-installed dowel bars were subjected to the tensile and shear stresses. However, the mechanical model was not proposed. Therefore, in this study, the previous model was modified to apply to the mechanical behavior under the shear and compressive normal stresses.

Section 2 describes the outline of the test, Section 3 explains the modified model, Section 4 discusses the model accuracy, and finally, Section 5 describes the conclusions.
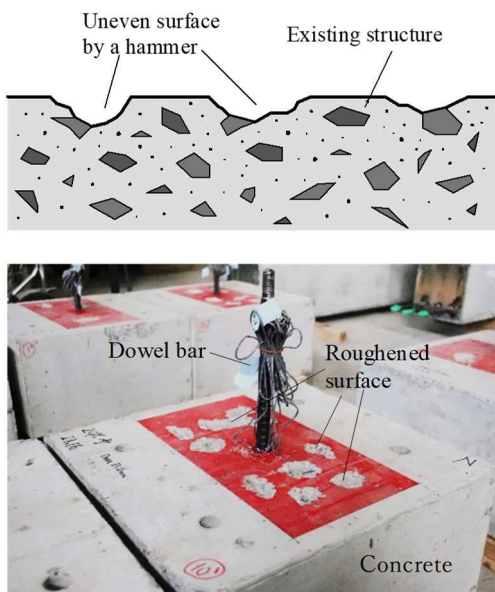

Fig. 1: Examples of interfaces. [1-2]

2 OUTLINE OF LOADING TEST

The previous test results [1] were used to verify the accuracy of the modified model. Therefore, the outline of the shear loading tests is briefly explained in this section.

2.1 Test parameters

The test parameters are listed in **Table 1**.

The test parameters were the diameter of the anchor bolt d_d, the roughness ratio r_{rc}, and the normal stress. The d_d and r_{rc} were set to 13, 16, 19 mm and 0.1, 0.2, 0.3, respectively.

The r_{rc} is obtained by the following equation.

$$r_{rc} = \frac{A_{hrc}}{A_j} \qquad (1)$$

where A_j and A_{hrc} are the interface area and the horizontal projection area of the uneven surface, respectively.

Table 1: Test parameters.

Specimen ID	σ_0 or r_N	r_{rc}		Anchor bar			Conc. & grout	
		Tar.	Mea.	d_d	f_y	E_s	f_c	f_g
D13R01C048	−0.48	0.1	0.115	13	403	174	22.5	68.0
D13R02C048	−0.48	0.2	0.206	13	403	174	20.1	69.2
D13R03C048	−0.48	0.3	0.316	13	403	174	22.5	68.0
D16R01C048	−0.48	0.1	0.107	16	387	175	20.1	69.2
D16R02C048	−0.48	0.2	0.190	16	387	175	20.1	69.2
D16R03C048	−0.48	0.3	0.302	16	387	175	20.1	69.2
D13R01T000	0.00	0.1	0.098	13	381	171	23.0	65.6
D13R01T033	0.33	0.1	0.106	13	381	171	23.0	65.6
D13R01T066	0.66	0.1	0.107	13	381	171	23.0	65.6
D13R02T000	0.00	0.2	0.194	13	381	171	23.0	65.6
D13R02T033	0.33	0.2	0.210	13	381	171	23.0	65.6
D13R02T066	0.66	0.2	0.199	13	381	171	23.0	65.6
D13R03T000	0.00	0.3	0.300	13	381	171	23.0	65.6
D13R03T033	0.33	0.3	0.318	13	381	171	23.0	65.6
D13R03T066	0.66	0.3	0.304	13	381	171	23.0	65.6
D16R01T000	0.00	0.1	0.093	16	387	175	20.8	62.9
D16R01T033	0.33	0.1	0.094	16	387	175	20.8	62.9
D16R01T066	0.66	0.1	0.106	16	387	175	20.8	62.9
D16R02T000	0.00	0.2	0.196	16	387	175	20.8	62.9
D16R02T033	0.33	0.2	0.199	16	387	175	20.8	62.9
D16R02T066	0.66	0.2	0.210	16	387	175	20.8	62.9
D16R03T000	0.00	0.3	0.301	16	387	175	20.8	62.9
D16R03T033	0.33	0.3	0.294	16	387	175	20.8	62.9
D16R03T066	0.66	0.3	0.292	16	387	175	20.8	62.9
D19R01T000	0.00	0.1	0.095	19	391	176	23.0	65.6
D19R01T033	0.33	0.1	0.102	19	391	176	23.0	65.6
D19R01T066	0.66	0.1	0.096	19	391	176	23.0	65.6
D19R02T000	0.00	0.2	0.215	19	391	176	23.0	65.6
D19R02T033	0.33	0.2	0.203	19	391	176	23.0	65.6
D19R02T066	0.66	0.2	0.204	19	391	176	23.0	65.6
D19R03T000	0.00	0.3	0.307	19	391	176	23.0	65.6
D19R03T033	0.33	0.3	0.304	19	391	176	23.0	65.6
D19R03T066	0.66	0.3	0.304	19	391	176	23.0	65.6

d_d [mm]: the diameter of anchor bar. f_y [N/mm^2] and E_s [kN/mm^2]: the yield strength and Young's modulus of dowel bar, respectively.

The compressive normal stress was set to −0.48 N/mm^2. For the tensile normal stress, the tensile ratio r_N, which is the ratio of the stress to the yield strength of anchor bolt, was used; and, set to 0.00, 0.33, and 0.66.

The material properties of the dowel bar, concrete, and grout are also listed in **Table 1**. The concrete used for the specimens was $f_c = 20$ N/mm^2; and, the material tests were based on JIS standards [17,18]. Here, the hole diameter $d_h = 16$, 22, and 25 mm for $d_d = 13$, 16, and 19 mm, respectively. Young's modulus of concrete $E_c = 17.4$, 21.8, 17.5 and 16.4 kN/mm^2 for $f_c = 22.5$, 20.1, 23.0 and 20.8 N/mm^2, respectively. Young's modulus of grout $E_g = 25.9$, 27.2, 26.4 and 24.4 kN/mm^2 for $f_g = 68.0$, 69.2, 65.6 and 62.9 N/mm^2, respectively.

2.2 Test specimen

The outline of the shear loading test is shown in **Fig. 2** (a). The specimens consisted of concrete and mortar blocks with dimensions of 440 mm × 460 mm × 250 mm and 375 mm × 200 mm × 190 mm, respectively. Plywood was used for the formwork of specimen. In addition, the concrete was cast vertically; therefore, the interface was smooth and greased. The effect of friction was low. After curing for 28 days, the surfaces were roughened by using a hammer. The anchor bolts were then adhered by using a diamond core drill and epoxy adhesive.

2.1 Shear loading test

The loading setup was used shown in **Fig. 2** (b). One 500-kN hydraulic jack was used for shear loading. In addition, two 150-kN screw jacks were used for normal stress loading. Four displacement sensors were used to measure the slip δ and opening ω. The measured ω was required for a PID (proportional–integral–derivative) auto-control system. With PID auto-control, the surface moved horizontally during shear loading and the normal stress was maintained at the target value. A static shear load was applied to the specimens. The load cycle was ±0.125, ±0.25, ±0.50, ±1.0, ±1.5, ±2.0, ±3.0, ±4.0, ±6.0, and ±8.0 mm.
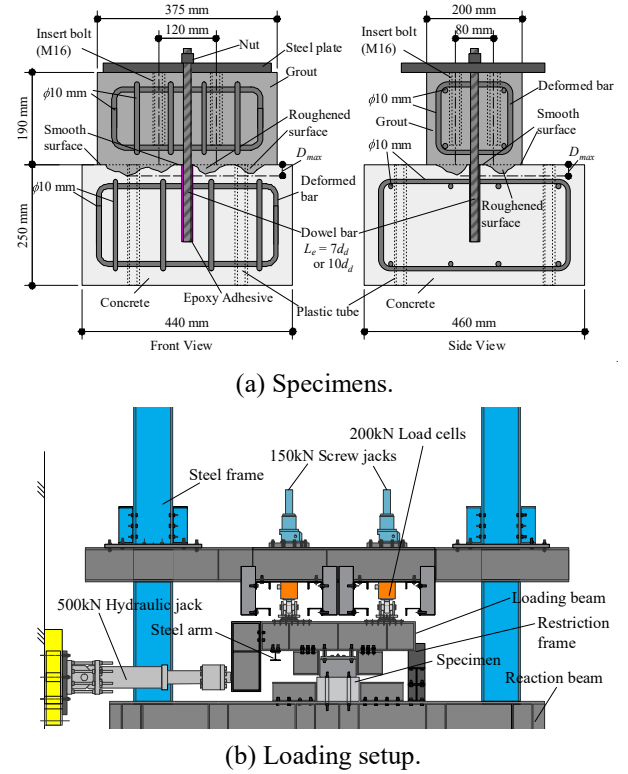

(a) Specimens.

(b) Loading setup.

Fig. 2: Outline of shear loading test.

3 MODIFIED MODEL

The authors proposed the cyclic model of the interface with a dowel bar and a roughened surface. In this section, the modification of the model is explained. In addition, the outlines of the original model are briefly explained.

3.1 Dowel model

The dowel model, which has been proposed in previous studies, was used in the modified model. **Fig. 3** shows a picture of the dowel model. In **Fig. 3**, the σ_b is the bearing stress of concrete, M_s is the full plastic bending moment at the plastic hinge, and σ_t is the tensile stress of the anchor bolt by a catenary action. [11-14]

The shear force Q_d is expressed as follows:

$$Q_d = q_s + q_B + q_T^S \qquad (2)$$

where q_s is the shear force caused by the bending moment of the plastic hinge, q_B is the bearing stress, and q_T^S is the shear force by the catenary action. These stresses can be calculated by using M_s, σ_b, and σ_t, respectively.
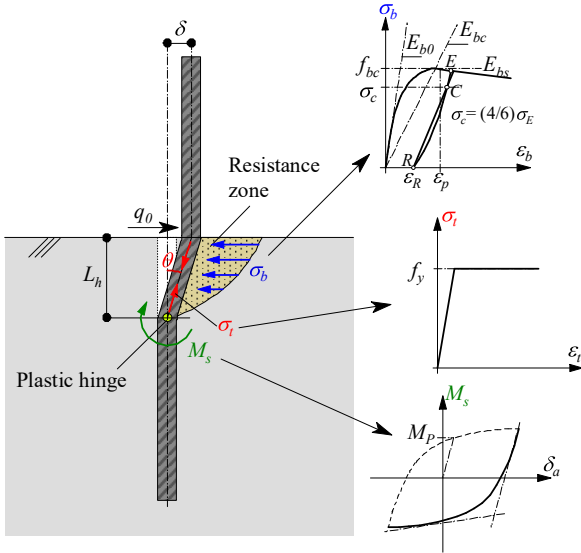
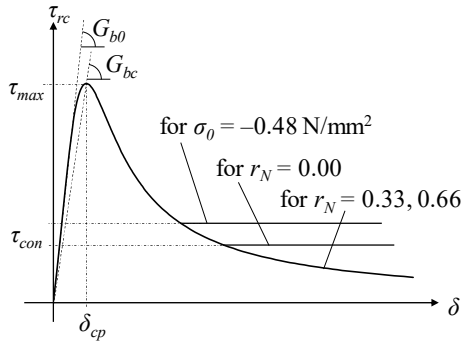**Fig. 3:** Image of the dowel model. [11-14]

Fig. 4: Envelope curve for roughened surface. [2]

3.2 Modified roughened surface model

In the previous study [2], the authors constructed the original model for the roughened surface. The original model can be applied to the specimens subjected to the tensile and shear stresses. In this study, the model was improved to estimate the behavior under the compressive normal stress.

3.2.1 Envelope curve

The following equation was used to model the envelope curve. [2]

$$\tau_{rc} = \frac{G_{b0} \cdot \delta}{1 + \left(\frac{G_{b0}}{G_{bc}} - 2\right)\left(\frac{\delta}{\delta_{cp}}\right) + \left(\frac{\delta}{\delta_{cp}}\right)^{\beta}} \quad (3)$$

where G_{b0} and G_{bc} are the initial stiffness and

angle of the line passing through the original and peak points, respectively. This equation was constructed using the Saenz model [19]. G_{b0} and δ_{cp} are set to 6.9 N/mm²/mm and = 0.50 mm, respectively. [2] In the Saenz model [18], $\beta = 2$ was employed. In this study, to express the stress-softening behavior of the roughened surface, the modified β was used as follows.

$$\beta = 3.5 \cdot r_N + 2.5 \geq 2.0 \quad (4)$$

Here, for the specimen subjected to the compressive normal stress, σ_0 is used instead of r_N.

Moreover, for the specimen with $\sigma_0 = -0.48$ N/mm² and $r_N = 0.00$, Q converged to a constant value. Therefore, τ_{con}, that is the constant shear stress after softening, is used; and, expressed by the following equation:

$$\tau_{con} = \begin{cases} -\sigma_0 \text{ for the comp. stress} \\ 0.3 \text{ for } r_N = 0.00 \\ 0.0 \text{ for } r_N > 0.00 \end{cases} \quad (5)$$

These values are obtained from the average stress with $\delta = 2$–6 mm.

Furthermore, the shear strength formula was proposed. [2] In the equation, the uneven surface was considered as a cone; and, with based on the previous study, the shear strength τ_{max} was expressed by vertical projection area of the uneven surface and the value of the exponent of f_c. Then, the value of $\tau_{max,p}$, that is the maximum shear stress on the positive side, is calculated by the following equation:

$$\tau_{max,p} = \left(\frac{r_{rc}D_{max}}{3\sqrt{\pi}} f_c^{0.24} + 0.13\right) \\ \times (1 - N) \quad (6)$$

where D_{max} is 12.6 mm, which is the average value of the specimens. N is the value of r_N or σ_0. To consider the effect by the normal stress, the function of $(1-N)$ is employed.

The minimum shear force on the negative side is calculated as follows:

$$\tau_{max,n} = 0.9 \times \tau_{max,p} \quad (7)$$

3.2.2 Unloading behavior

The cyclic model is illustrated in **Fig. 5**. Points B and C are the start and end points of the unloading curve, respectively. Point Z

represents the intersection of the unloading and reloading curves. The parabolic function was used for the unloading behavior. This model passes through Points B and C in **Fig. 5**. δ_B and δ_C are the shear displacements of Points B and C, respectively; and, are expressed as follows.

$$\delta_C = 0.9 \cdot \delta_B \tag{8}$$

Here, Point C is the vertex of the parabolic function, therefore, the following equations are obtained for the unloading behavior.

$$\tau_{rc} = \gamma(\delta - \delta_c)^2 \tag{9}$$

$$\gamma = \frac{\tau_B}{(0.1 \cdot \delta_B)^2} \tag{10}$$

3.2.3 Reloading behavior

As well, the reloading behavior starts from the original Point O; and, the behavior is the linear function. Point Z, that is the intersection of the unloading and reloading behaviors, is expressed as follows:

$$\tau_Z = \begin{cases} 0.5\tau_B \text{ for } r_N = 0.00\sim0.66 \\ \frac{2}{3}\tau_B \text{ for } \sigma_0 = -0.48 \text{ N/mm}^2 \end{cases} \tag{11}$$

where, τ_Z is the shear stress of Point Z. In this study, the lower equation of Eq. (11) was added for the compressive normal stress. The reloading behavior τ_{rc} can be obtained as follows:

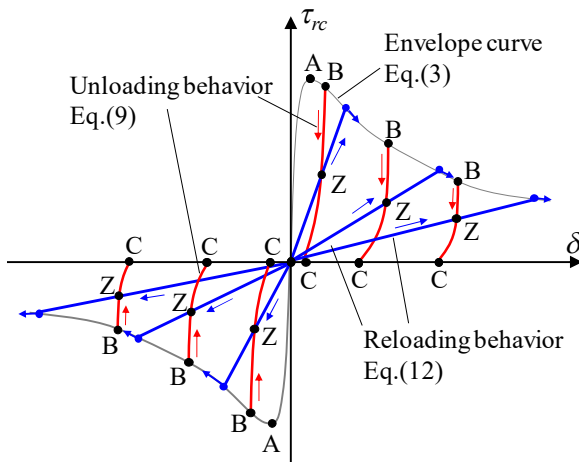$$\tau_{rc} = \frac{\tau_Z}{\delta_Z} \cdot \delta \tag{12}$$

After the reloading line crosses the envelope curve, τ_{rc} is expressed by Eq. (3).

3.2.4 Coefficient for effect of d_d

As mentioned in the previous paper [2], when d_d was smaller, the opening was wider; therefore, for the specimen with d_d = 13 mm, the previous model overestimated the test results. **Fig. 6** shows the relationship between α and d_d. Here, α is the safety factor, which can be obtained by dividing Q_{max} by Q_{cal}. According to **Fig. 6**, the medians for d_d = 16 and 19 mm are almost the same. Whereas the median for d_d = 13 mm is smaller than that for d_d = 16 and 19 mm.

Hence, in this study, K_α, that is the coefficient to evaluate the effect of d_d, was used and is described as the follows:

$$K_\alpha = \begin{cases} 0.05d_d + 0.2 \text{ for } 13 \leq d_d < 16 \\ 1.0 \text{ for } d_d \geq 16 \end{cases} \tag{13}$$

From the above, the analytical shear load Q_{Ana} is expressed by the following equation.
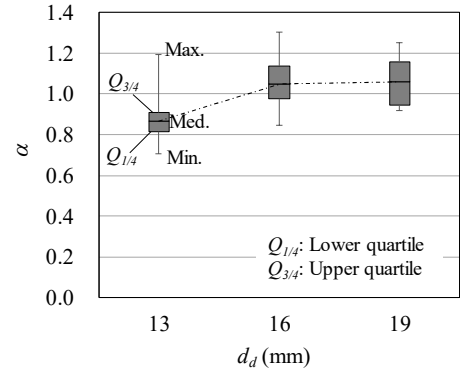
$$Q_{Ana} = Q_{d,ave} + Q_{rc} \tag{14}$$

Fig. 6: Relation between α and d_d.
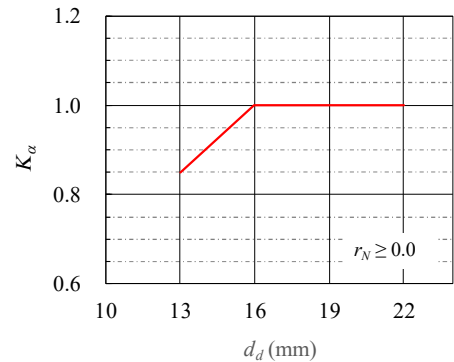

Fig. 7: Relation between K_α and d_d.

Fig. 5: Cyclic rules for the roughened surface.

5

$$Q_{rc} = K_\alpha \times A_j \times \tau_{rc} \qquad (15)$$

where $Q_{d,ave}$ is obtained by Eq. (2), with $\delta = 0.46$ mm, which is the average shear displacement during Q_{max}.

4 DISCUSSION

This section compares the analytical values of the proposed model with the test results. In addition, the failure mode was briefly explained.

4.1 Test results

Fig. 8 shows the failure mode of the specimens. As shown in **Fig. 8**, the bearing damage was confirmed around the dowel bars and uneven surfaces. Similar damage was also observed in the other specimens. Therefore, the specimens were failed by dowel action and bearing stress on the roughened surface.

4.2 Q–δ curves

Figs. 9–11 show the Q-δ curves for $d_d = 13$, 16, and 19 mm, respectively. The blue lines are the calculated results of the dowel model.

4.2.1 $d_d = 13$ mm

From **Fig. 9** (i)-(iv) with $r_{rc} = 0.1$, the proposed models reasonably estimate the four test results. For $r_N = 0.33$ and 0.66, the dowel models are corresponding with the test results after $\delta = 2$ mm.
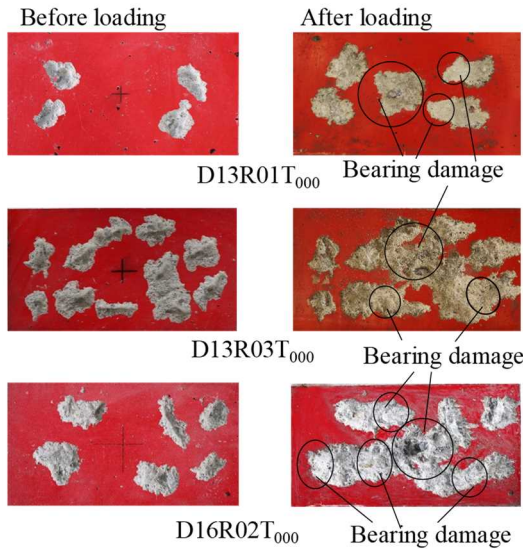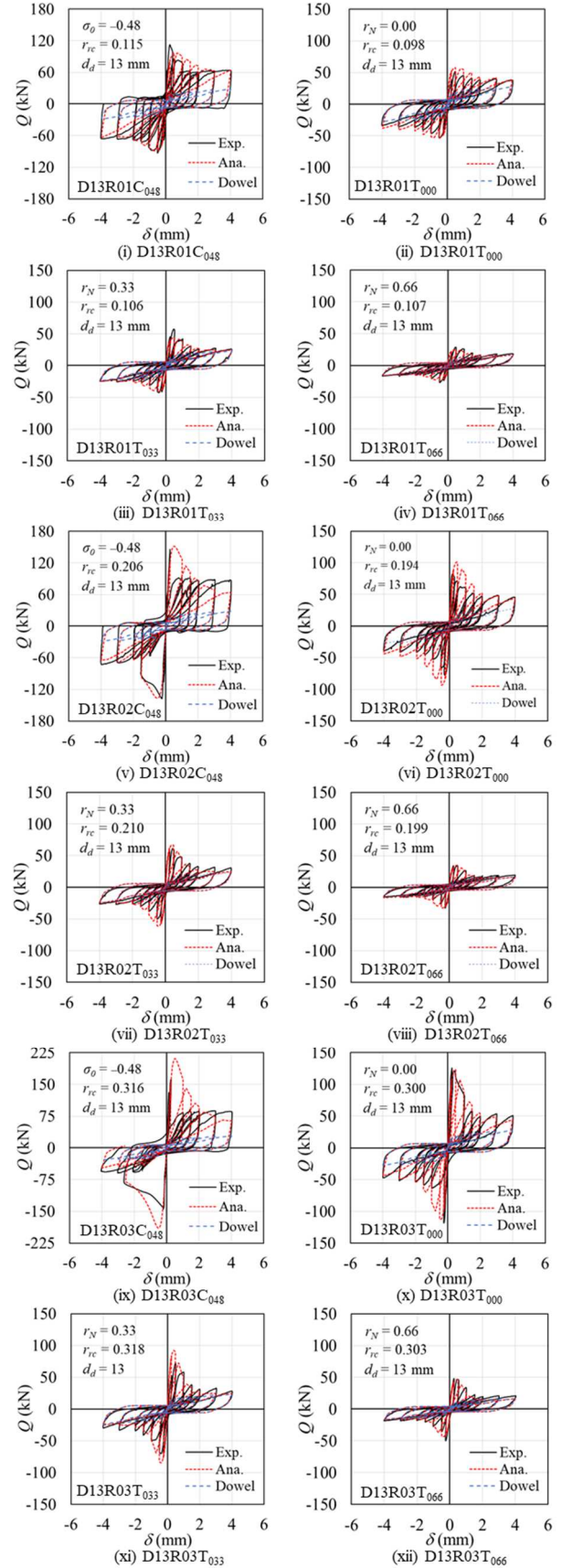
Fig. 8: Failure modes.

Fig. 9: Q-δ curves for $d_d = 13$ mm.

Therefore, when the interfaces are subjected to the tensile stress, only the dowel bars resist to the shear force in the large displacement region.

Focusing on the results of D13R02C$_{048}$ and D13R03C$_{048}$ in **Fig. 9** (v) and (ix), the proposed model cannot estimate the test result from δ = +0.25 mm to +1 mm. In these specimens, the large slip behavior was observed on the negative side. Therefore, after δ = +0.25 mm, the shear force was smaller than the other specimens. Hence, the model could not estimate the irregular behavior. In addition, the large slip behavior was observed for the specimens with σ_0 = –0.48 N/mm^2. Expect for these two specimens, the proposed model can reasonably estimate the envelope curve, unloading behavior, and the reloading behavior of the test results.

4.4.2 d_d = 16 mm

Fig. 10, that shows the results of the specimen with d_d = 16 mm, is observed. Focusing on the specimens with σ_0 = –0.48 N/mm^2, the large slips that were confirmed in **Fig. 9** are not observed. Thus, as the d_d becomes smaller, the dowel effect decreases; therefore, the specimens failed brittle. However, the model overestimates the peak forces for the specimens with σ_0 = –0.48 N/mm^2 in **Fig. 10** (v) and (ix). As shown in **Fig. 9**, for some of the tests, the model could not estimate well. However, for most of the specimens, the analytical results by the model are in good agreement with the test results.

4.2.3 d_d = 19 mm

Finally, **Fig. 11** is focused. The specimens with d_d = 19 mm were only subjected to the tensile normal and shear stresses; thus, the compressive normal stress was not applied.

As well as the specimens with r_N = 0.00-0.66 in **Figs. 9** and **10**, the proposed model reasonably estimates the test results.
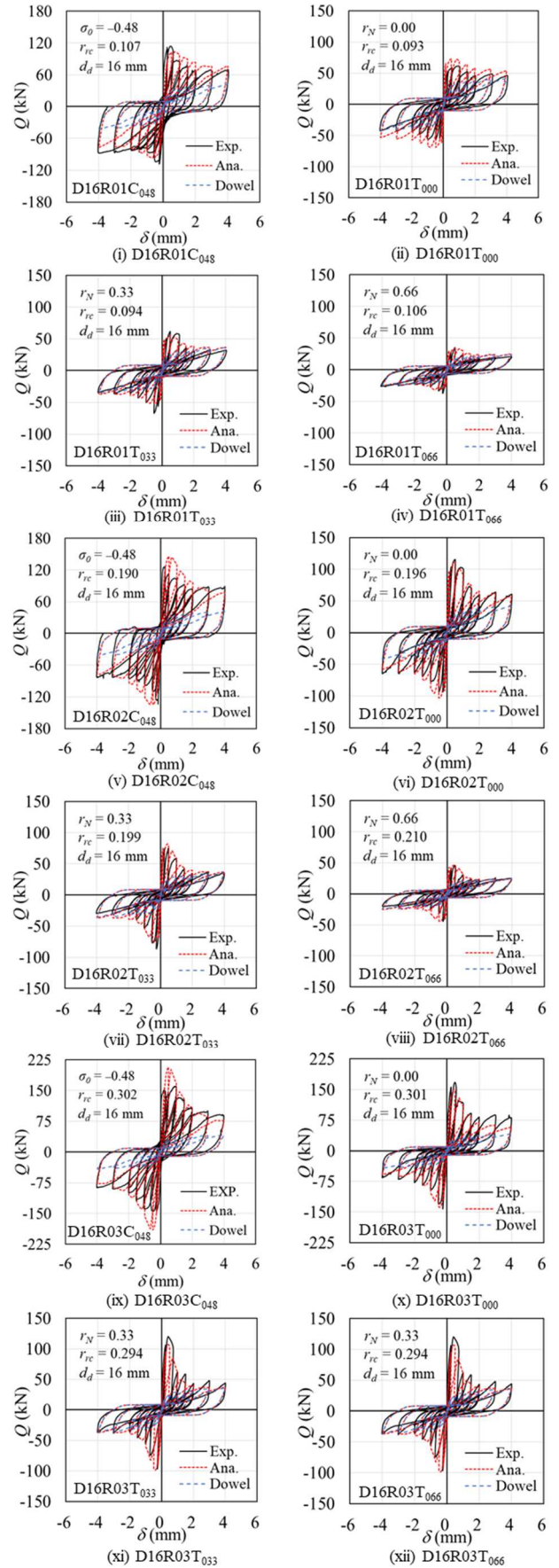

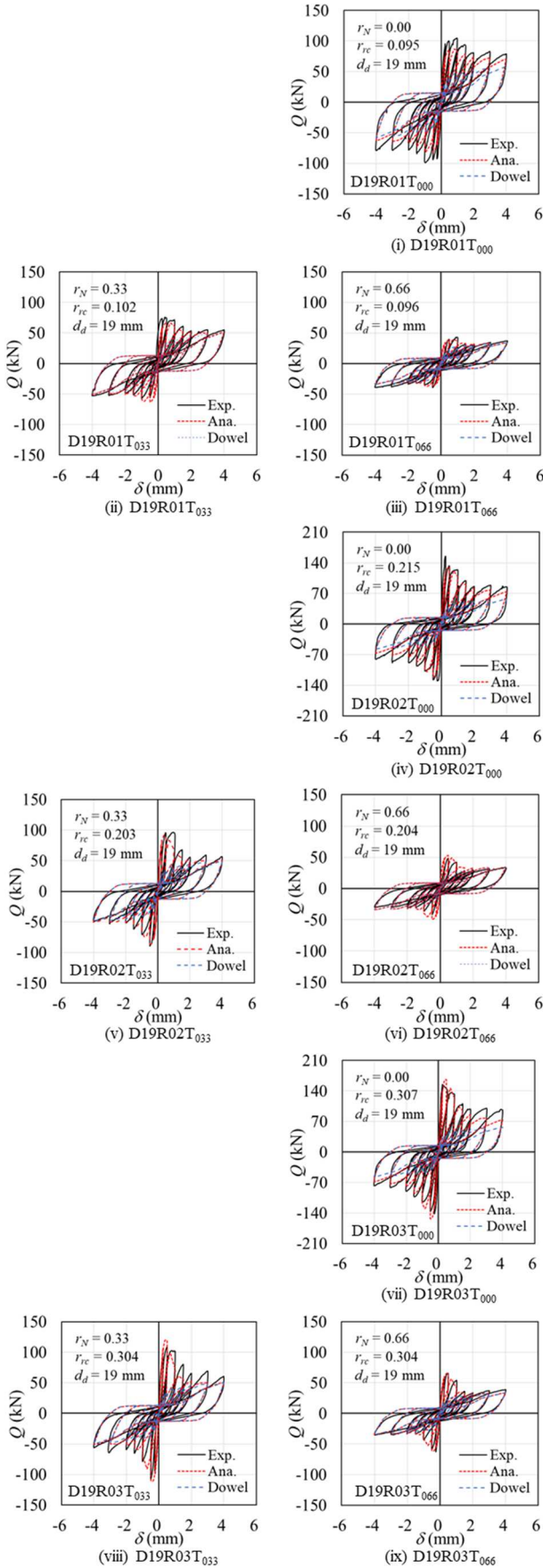**Fig. 10**: Q-δ **curves** for d_d = 16 mm.

Fig. 11: Q-δ **curves** for $d_d = 19$ mm.

As mentioned earlier, except for the irregular behavior, the modified model is useful for estimating the mechanical behavior of the interface with the post-installed anchor and the roughened surface subjected to the normal and shear stresses.

4.2.4 Dowel action

In the section, the blue lines of **Figs. 9-11**, which indicate the result of dowel action, are focused. In all figures, when δ is smaller, the gaps between the test results and the dowel model are larger. Therefore, the effect of the roughened surface on the shear resistance is greater. As δ increased, the effect of the dowel bar became significant. Moreover, when the surface was subjected to the compressive normal stress, the effect of the dowel bar became less significant than that of the tensile normal stress.

4.3 Model to test shear force ratio

Table 2 lists the test to model shear force ratio R_{t2m}. As mentioned in Section 4.2, the irregularities were confirmed for the specimens with $d_d = 13$ mm and $\sigma_0 = -0.48$ N/mm^2; and, in these case, the analytical results did not agree well with the test results. Thus, the R_{t2m} of D13R02C$_{048}$ and D13R03C$_{048}$ with $\delta = +1$ mm are 0.59 and 0.52, respectively. These values are lower than the other results. On contrast, the R_{t2m} of D16R02T$_{066}$ and D16R03T$_{000}$ with $\delta = +3$ mm are 1.40, that is the highest of all. However, the average values of R_{t2m} are 0.91-1.12. Therefore, from the discussion in this section, it is concluded that the model can reasonably estimate the test results.

5 CONCLUSIOTN

In this study, the mechanical behavior of the interfaces with post-installed dowel bars and roughened surfaces by a vibratory hammer has been investigated. Moreover, the previous model [2] was modified to estimate the interfaces subjected to the compressive normal and shear stresses. The results of this study are described below.

Table 2: Test-to-model shear force ratio R_{t2m}.

Specimen ID	δ on positive side			δ on negative side		
	+1.0	+2.0	+3.0	−1.0	−2.0	−3.0
D13R01C$_{048}$	0.87	0.84	0.99	1.00	1.00	1.06
D13R02C$_{048}$	0.59	1.00	1.29	0.88	0.99	1.03
D13R03C$_{048}$	0.52	0.88	1.19	-	1.01	1.31
D16R01C$_{048}$	0.86	0.82	0.90	0.91	1.02	1.14
D16R02C$_{048}$	0.79	0.84	1.09	0.79	0.91	1.05
D16R03C$_{048}$	0.96	1.00	1.07	0.88	0.94	1.06
D13R01T$_{000}$	0.83	0.88	0.96	0.90	0.86	0.87
D13R01T$_{033}$	1.15	1.00	1.13	0.87	0.92	1.04
D13R01T$_{066}$	1.22	1.05	1.16	0.99	0.89	1.09
D13R02T$_{000}$	0.76	0.91	1.00	0.69	0.80	0.85
D13R02T$_{033}$	1.05	1.18	1.28	1.05	1.18	1.28
D13R02T$_{066}$	1.10	1.15	1.18	0.56	0.89	0.66
D13R03T$_{000}$	0.92	0.92	1.11	0.75	1.00	1.07
D13R03T$_{033}$	1.17	1.15	1.34	1.02	1.22	1.32
D13R03T$_{066}$	1.31	1.22	1.32	1.08	1.01	1.17
D16R01T$_{000}$	0.88	0.79	0.86	0.83	0.82	0.87
D16R01T$_{033}$	1.19	0.81	0.91	1.05	0.93	0.99
D16R01T$_{066}$	0.83	0.74	0.82	0.92	0.95	1.03
D16R02T$_{000}$	1.10	0.91	1.02	0.89	1.04	1.17
D16R02T$_{033}$	1.04	0.87	1.02	0.96	0.76	0.82
D16R02T$_{066}$	1.08	1.20	1.40	0.93	1.20	1.13
D16R03T$_{000}$	1.08	1.20	1.40	0.93	1.20	1.13
D16R03T$_{033}$	1.01	1.10	1.31	0.92	0.92	1.02
D16R03T$_{066}$	0.87	0.84	0.93	0.56	0.80	0.86
D19R01T$_{000}$	1.24	1.10	1.09	1.22	1.18	1.21
D19R01T$_{033}$	1.15	1.05	1.10	0.96	0.95	1.05
D19R01T$_{066}$	1.16	0.95	1.04	0.98	1.05	1.14
D19R02T$_{000}$	1.14	1.06	1.15	1.03	1.16	1.16
D19R02T$_{033}$	1.41	1.06	1.17	0.57	1.01	1.07
D19R02T$_{066}$	1.05	0.92	0.92	0.93	0.93	0.92
D19R03T$_{000}$	1.08	1.17	1.29	0.98	1.13	1.12
D19R03T$_{033}$	1.39	1.27	1.39	1.10	1.14	1.29
D19R03T$_{066}$	1.30	1.04	1.13	1.06	1.04	1.00
Average	1.03	1.00	1.12	0.91	1.00	1.06

1) In order to apply the previous model [2] to the compressive normal stress, the envelope curve and the softening coefficient β, which was shown in Eq. (4), were modified. Furthermore, the constant shear stress after softening τ_{con}, which was shown in Eq. (5), was modified.

2) Point Z has been improved for estimating the reloading behavior of the specimen under compressive normal stress.

3) As the diameter of dowel bar d_d was smaller, the opening width of interfaces was wider. [1-2] To consider this effect, the coefficient K_α was added to the previous model.

4) For D13R02C$_{048}$ and D13R03C$_{048}$ with $d_d =$ 13 mm and $\sigma_0 = -0.48$ N/mm^2, the large slip behavior was observed on the negative loading. Therefore, the model could not accurately estimate these test results.

5) With the increase of δ, the effect of dowel bar was intensified; whereas, under the compressive normal stress, it became insignificant.

6) When comparing the analytical results with the test results, although some discrepancies were confirmed, the modified model could reasonably estimate the test results for most of the specimens. The average values of the ratio between the model and test results were 0.91-1.12.

REFERENCES

[1] Takase, Y. and Yamada, T., 2022. Shear strengths of joints with roughened concrete surfaces and post-installed dowel bars subjected to normal and shear stresses for seismically retrofitted structures. *Structures*. 45:900–911.

[2] Yamada, T., Takase, Y. and Abe, T., 2023. Cyclic Behavior of interfaces for seismically retrofitted RC buildings, *Journal of Advanced Concrete Technology*. 45:900-911.

[3] Mattock, A. H. and Hawkins, N. M., 1972, Shear transfer in reinforced concrete recent re-search, *PCI Journal*. 17:55–75.

[4] Walraven, J. C., 1981. Fundamental analysis of aggregate interlock. *Journal of Structural Division*. *ASCE*, 107(11): 2245–2270.

[5] Walraven, J. C. and Reinhardt, H. W., 1981. Theory and experiments on the mechanical behavior of cracks in plain and reinforced concrete subjected to shear loading. *Heron*. 26(1A):1–68.

[6] Bujadaham, B. and Maekawa, K., 1992. Qualitative studies on mechanisms of stress transfer across cracks in concrete. *Proceedings of JSCE*. 451(V-17): 265–275.

[7] Bujadaham, B. and Maekawa, K., 1992. The universal model for stress transfer

across cracks in concrete. *Proceedings of JSCE*. 451(V-17):277–287.

[8] Friberg, B. F., 1938. Design of dowels in the transverse joints of concrete pavements. *Proceedings of American Society of Civil Engineer*. 64(9):1809–1828.

[9] Vintzēleou, E. N. and Tassios, T. P., 1986. Mathematical models for dowel action under monotonic and cyclic conditions. *Magazine of Concrete Research*. 38(134): 13–22.

[10] Sorensen, J. H., Hoang, L. C., Olesen, J. F. and Fischer, G., 2017. Testing and modeling dowel and catenary action in rebars crossing shear joints in RC. *Engineering Structures*. 145: 234–245.

[11] Takase, Y., 2019. Testing and modeling of dowel action for a post–installed anchor subjected to combined shear and tensile forces. *Engineering Structures*. 195:551-558.

[12] Takase, Y., Wada, T., Ikeda, T., Shinohara, Y., 2013. Mechanical model of adhesive post–installed anchor subjected to cyclic shear force. *Proceedings of Fracture Mechanics of Concrete and Concrete Structures*. 1727–1736.

[13] Matsunaga, K., Takase, Y. and Abe, T., 2021. Modeling of dowel action for cast–in and post–installed anchors considering bond property. *Engineering Structures*. 245:112773.

[14] Matsunaga, K., Takase, Y., Abe, T., Orita, G. and Ando, S., 2022. Property of cement based adhesive anchor constructed below zero and estimating of mechanical behavior. *Journal of Structural and Construction Engineering, Transactions of AIJ*. 87(796):556-566.

[15] Musya, U., Katagiri, Y., Takase, Y., Abe, T., Sakamoto, K., Hiwatashi, T. and Katori, K., 2019. Bearing strength formula of roughened concrete considering vertical projection area. *Journal of Advanced Concrete Technology*. 17:309-318.

[16] Katagiri, Y., Takase, Y., Abe, T., Sakamoto, K., Hiwatashi, T. and Katori, K., 2019. Mechanical model of roughened concrete of existing members for shear failure mode. *Proceedings of Fracture mechanics of Concrete and Concrete Structures*. 235482.

[17] JIS, 2011. Metallic materials – Tensile testing – Method of test at room temperature. *Japanese Industrial Standards*. 2241. (in Japanese)

[18] JIS, 2018. Method of test for compressive strength of concrete. *Japanese Industrial Standards*. 1108. (in Japanese)

[19] Saenz, L. P., 1964. Discussion of equation for stress - strain curve of concrete, by Desayi P and Krishnan S. *ACI Journal*. 61(9):1229–1235.